Measurement of the branching fraction of the decay $B_s^0 \to K_S^0 K_S^0$

R. Aaij *et al.*[*]
(LHCb Collaboration)

(Received 20 February 2020; accepted 9 June 2020; published 31 July 2020)

A measurement of the branching fraction of the decay $B_s^0 \to K_S^0 K_S^0$ is performed using proton–proton collision data corresponding to an integrated luminosity of 5 fb^{-1} collected by the LHCb experiment between 2011 and 2016. The branching fraction is determined to be $\mathcal{B}(B_s^0 \to K_S^0 K_S^0) = [8.3 \pm 1.6(\text{stat}) \pm 0.9(\text{syst}) \pm 0.8(\text{norm}) \pm 0.3(f_s/f_d)] \times 10^{-6}$, where the first uncertainty is statistical, the second is systematic, and the third and fourth are due to uncertainties on the branching fraction of the normalization mode $B^0 \to \phi K_S^0$ and the ratio of hadronization fractions f_s/f_d. This is the most precise measurement of this branching fraction to date. Furthermore, a measurement of the branching fraction of the decay $B^0 \to K_S^0 K_S^0$ is performed relative to that of the $B_s^0 \to K_S^0 K_S^0$ channel, and is found to be $\frac{\mathcal{B}(B^0 \to K_S^0 K_S^0)}{\mathcal{B}(B_s^0 \to K_S^0 K_S^0)} = [7.5 \pm 3.1(\text{stat}) \pm 0.5(\text{syst}) \pm 0.3(f_s/f_d)] \times 10^{-2}$.

DOI: 10.1103/PhysRevD.102.012011

I. INTRODUCTION

Flavor-changing neutral current processes, especially neutral B meson decays to kaons and excited kaons, can be used as probes of the Standard Model and of the Cabibbo-Kobayashi-Maskawa (CKM) unitarity triangle angle $\beta_{(s)}$. While decays such as $B_{(s)}^0 \to K^{*0}\bar{K}^{*0}$, $B_s^0 \to K^{*0}\bar{K}^0$, and $B^0 \to K^+K^-$ have already been measured at the LHC [1–4], decays of b hadrons to final states containing only long-lived particles, such as K_S^0 mesons or Λ baryons, have never before been reported in a hadronic production environment. A measurement of the branching fraction of $B_s^0 \to K^0\bar{K}^0$ decays can be used as input to future SM predictions, and is a first step toward a time-dependent measurement of CP violation in this channel using future LHC data.

In the Standard Model, the decay amplitude of $B_s^0 \to K^0\bar{K}^0$ is dominated by $b \to s\bar{d}d$ loop transitions with gluon radiation, while other contributions, including color singlet exchange, are suppressed to the level of 5% [5] in the decay amplitude. Predictions of this branching fraction within the SM lie in the range $(15\text{–}25) \times 10^{-6}$ [6–9], with calculations relying on a variety of theoretical approaches such as soft collinear effective theory, QCD factorization, and perturbative leading-order and next-to-leading-order QCD. Beyond the Standard Model, possible contributions from new particles or couplings [5,10–13] can be probed by improved experimental precision on the branching fraction measurement.

The decay $B_s^0 \to K^0\bar{K}^0$ was first observed by the Belle collaboration in 2016 [14]. The branching fraction was determined to be $\mathcal{B}(B_s^0 \to K^0\bar{K}^0) = (19.6^{+5.8}_{-5.1} \pm 1.0 \pm 2.0) \times 10^{-6}$, where the first uncertainty is statistical, the second systematic and the third due to the uncertainty of the total number of produced $B_s^0 - \bar{B}_s^0$ pairs. The related decay $B^0 \to K^0\bar{K}^0$ has a branching fraction of $(1.21 \pm 0.16) \times 10^{-6}$ [15–17] in the world average.

This paper presents measurements of the branching fraction of $B_{(s)}^0 \to K_S^0 K_S^0$ decays using proton-proton collision data collected by the LHCb experiment at center-of-mass energies $\sqrt{s} = 7$, 8, or 13 TeV. The $B_{(s)}^0 \to K_S^0 K_S^0$ branching fraction is assumed to be half of the $B_{(s)}^0 \to K^0\bar{K}^0$ branching fraction, as the $K^0\,\bar{K}^0$ final state is CP even. These $B_{(s)}^0$ branching fractions are determined relative to the $B^0 \to \phi K_S^0$ branching fraction, where the notation ϕ is used for the $\phi(1020)$ meson throughout. This normalization mode has a corresponding branching fraction equal to half of $\mathcal{B}(B^0 \to \phi K^0) = (7.3 \pm 0.7) \times 10^{-6}$ [18,19], and is chosen for its similarity to the signal mode. Despite the smaller branching fraction, the yield of the normalization mode is much larger than that of the signal mode, because the near-instantaneous ϕ decay can be reconstructed more efficiently than a long-lived K_S^0, and because for LHCb the production fraction of B^0 mesons is approximately four times that of B_s^0 mesons. [20,21]. Throughout this paper, the decays $B_{(s)}^0 \to K_S^0 K_S^0$ and $B^0 \to \phi K_S^0$ are reconstructed using the decays $K_S^0 \to \pi^+\pi^-$ and $\phi \to K^+K^-$.

[*]Full author list given at the end of the article.

The paper is structured as follows. A brief description of the LHCb detector as well as the simulation and reconstruction software is given in Sec. II. Signal selection and strategies to suppress background contributions are outlined in Sec. III. The models to describe the invariant-mass components, the fitting and the normalization procedure are introduced in Sec. IV. Systematic uncertainties are discussed in Sec. V. Finally, the results are summarized in Sec. VI.

II. LHCb DETECTOR

The LHCb detector [22,23] is a single-arm forward spectrometer covering the pseudorapidity range $2 < \eta < 5$, designed for the study of particles containing b or c quarks. The detector includes a high-precision tracking system consisting of a silicon-strip vertex detector (VELO) surrounding the pp interaction region [24], a large-area silicon-strip detector located upstream of a dipole magnet with a bending power of about 4Tm, and three stations of silicon-strip detectors and straw drift tubes [25,26] placed downstream of the magnet. The tracking system provides a measurement of momentum, p, of charged particles with a relative uncertainty that varies from 0.5% at low momentum to 1.0% at 200 GeV/c. The minimum distance of a track to a primary vertex (PV), the impact parameter (IP), is measured with a resolution of $(15 + 29/p_{\mathrm{T}})$ μm, where p_{T} is the component of the momentum transverse to the beam, in GeV/c. Different types of charged hadrons are distinguished using information from two ring-imaging Cherenkov detectors [27]. Photons, electrons and hadrons are identified by a calorimeter system consisting of scintillating-pad and preshower detectors, an electromagnetic calorimeter and a hadronic calorimeter. Muons are identified by a system composed of alternating layers of iron and multiwire proportional chambers.

The online event selection is performed by a trigger [28], which consists of a hardware stage, based on information from the calorimeter and muon systems, followed by a software stage, which applies a full event reconstruction. At the hardware trigger stage, events are required to contain a muon with high p_{T} or a hadron, photon or electron with high transverse energy in the calorimeters. In the software trigger, events are selected by a topological b-hadron trigger. At least one charged particle must have a large transverse momentum and be inconsistent with originating from any PV. A two- or three-track secondary vertex is constructed, which must have a large sum of the p_{T} of the charged particles and a significant displacement from any PV. A multivariate algorithm [29] is used for the identification of secondary vertices consistent with the decay of a b-hadron. This is used to collect both $B^0_{(s)} \to K^0_{\mathrm{S}}K^0_{\mathrm{S}}$ and $B^0 \to \phi K^0_{\mathrm{S}}$ decays. In addition to this topological trigger and algorithm, some $B^0 \to \phi K^0_{\mathrm{S}}$ decays are also collected using dedicated ϕ trigger requirements that exploit the topology of the $\phi \to K^+K^-$ decay and apply additional particle identification requirements to the charged kaons.

Simulation is required to model the effects of the detector acceptance and the imposed selection requirements. In simulation, pp collisions are generated using PYTHIA [30] with a specific LHCb configuration [31]. Decays of hadronic particles are described by EvtGen [32], in which final-state radiation is generated using PHOTOS [33]. The interaction of the generated particles with the detector, and its response, are implemented using the GEANT4 toolkit [34] as described in Ref. [35].

III. EVENT SELECTION

The decays $B^0_{(s)} \to K^0_{\mathrm{S}}K^0_{\mathrm{S}}$ and $B^0 \to \phi K^0_{\mathrm{S}}$ are reconstructed using the decay modes $K^0_{\mathrm{S}} \to \pi^+\pi^-$ and $\phi \to K^+K^-$.[1] The long-lived K^0_{S} mesons are reconstructed in two different categories, depending on whether the K^0_{S} meson decays early enough that the pions can be tracked inside the VELO, or whether the K^0_{S} meson decays later and its products can only be tracked downstream. These are referred to as *long* and *downstream* track categories, and are abbreviated as L and D, respectively. The K^0_{S} mesons reconstructed in the long track category have better mass, momentum and vertex resolution than the downstream track category. However, due to the boost of the B meson, the lifetime of the K^0_{S} meson, and the geometry of the detector, there are approximately twice as many K^0_{S} candidates reconstructed in the downstream category than in the long category, before any selections are applied.

This analysis is based on pp collision data collected by the LHCb experiment. Data collected in 2011 (2012) were recorded at a center-of-mass energy of 7 TeV (8 TeV), while in 2015 and 2016 the center-of-mass energy was increased to 13 TeV. Data recorded at center-of-mass energies of 7 and 8 TeV (Run 1) are combined and then treated separately from data recorded at 13 TeV (Run 2). Due to low trigger efficiency for B^0_s mesons decaying into two downstream K^0_{S} mesons, these are discarded from the analysis. Consequently, there are four data categories that are considered in the following—Run 1 LL, Run 1 LD, Run 2 LL and Run 2 LD—and measurements are performed separately in each of these data categories before being combined in the final fit.

Signal B^0_s or B^0 candidates are built in successive steps, with individual K^0_{S} candidates reconstructed first and then combined. The K^0_{S} candidates are constructed by combining two oppositely charged pions that meet certain requirements on the minimum total momentum and transverse momentum; on the minimum χ^2_{IP} of the K^0_{S} candidate with respect to the associated PV (where χ^2_{IP} is defined as the

[1]The inclusion of charge-conjugate processes is implied throughout the paper.

difference in the impact parameter χ^2 of a given PV reconstructed with and without the considered particle); on the maximum distance of closest approach (DOCA) between the two particles; and on the quality of the vertex fit. An event can have more than one PV, in which case the associated PV is defined as that with which the B candidate forms the smallest value of $\chi^2_{\rm IP}$. The invariant mass of K^0_S candidates constructed from long (downstream) tracks must be within 35 MeV/c^2 (64 MeV/c^2) of the known K^0_S mass [15]. The DOCA between the two K^0_S candidates is required to be smaller than 1 mm for the LL category and 4 mm for the LD category. Signal B^0_s or B^0 candidates are then formed by combining two K^0_S candidates that result in an invariant mass close to the known $B^0_{(s)}$ masses, discussed further below and in Sec. IV.

The normalization decay $B^0 \to \phi K^0_S$ is constructed in a similar way. The ϕ meson is constructed by combining two oppositely charged kaon candidates that result in an invariant mass within 50 MeV/c^2 of the nominal ϕ mass, as a first loose selection. Due to the vanishing lifetime of the ϕ meson, the charged kaon candidates are only reconstructed from long tracks, and thus all ϕ are reconstructed in the L category. The K^0_S meson of the normalization decay can be either L or D, so that the $B^0 \to \phi K^0_S$ decay has both LL and LD reconstructions.

The rest of the candidate selection process consists of a preselection followed by the application of a multivariate classifier, and then some additional selections are applied to further reduce combinatorial background. In the preselection, loose selection requirements are applied to remove specific backgrounds from other b-hadron decays and suppress combinatorial background. These backgrounds for the signal and normalization modes are discussed further below. Additional suppression of the combinatorial background is included using a final selection after the multivariate classifier is applied, where particle identification (PID) requirements are added such that all final-state particles must be inconsistent with the muon hypothesis based on the association of hits in the muon stations.

Possible background decays are studied using simulated samples. For the signal channel, these include: $B^0_{(s)} \to K^0_S\pi^+\pi^-$; $B^0_{(s)} \to K^0_S\pi^+K^-$ with kaon–pion misidentification; $B^0_{(s)} \to K^0_S K^+K^-$ with double kaon–pion misidentification; and $\Lambda^0_b \to pK^0_S\pi^-$ with proton–pion misidentification. Backgrounds from $K^0_L \to \pi^+\pi^-$ decays are negligible. Applying the K^0_S mass window requirement to the two-hadron system originating directly from a b-hadron decay reduces the background yields by a factor of 10 to 100, depending on the decay channel. To further suppress the contribution of these modes, a requirement on the distance along the beam axis direction (the z-direction) between the decay vertices of the K^0_S and B^0_s candidates, $\Delta z > 15$ mm, is applied to K^0_S candidates reconstructed from long tracks for both decay channels.

An additional background comes from the requirements used to identify K^0_S candidates, which may also select Λ baryons due to their long flight distance. The $\Lambda \to p\pi^-$ decays are excluded by changing the mass hypothesis of one pion candidate to the proton hypothesis, reconstructing the invariant mass, $m(p\pi^-)$, and tightening the pion PID requirement in an 8 MeV/c^2 mass window around the known Λ mass. This procedure is carried out for each pion from each K^0_S candidate, in both the signal and normalization channels.

For the normalization channel $B^0 \to \phi K^0_S$, the decays $B^0_{(s)} \to K^0_S h^{(\prime)+}h^{(\prime)-}$ with $h^{(\prime)\pm} = \pi^\pm, K^\pm$ are suppressed by requiring the invariant mass of the combination of the two final-state kaons to be close to the ϕ mass. The largest contributions are expected from the decay channel $B^0_s \to K^0_S\pi^+K^-$ with a fraction of about 1% compared to $B^0 \to \phi K^0_S$ decays. This is reduced to a negligible level by applying PID requirements to the kaon candidates. The partially reconstructed decays $B^0 \to \phi K^{*0}$ and $B^+ \to \phi K^{*+}$, with $K^{*0} \to K^0_S\pi^0$ and $K^{*+} \to K^0_S\pi^+$, share the same decay topology as the normalization channel when omitting the pion that originates from decay of the K^* resonance and have a higher branching fraction than the normalization decay. Due to the missing particle, the B candidates have a kinematic upper limit on their masses of about 5140 MeV/c^2. Therefore, the mass window to determine the yield of the normalization channel is set to $5150 < m(K^0_S K^+K^-) < 5600$ MeV/c^2 to fully exclude these contributions.

Further separation of signal from combinatorial background is achieved using the XGBoost implementation [36] of the boosted decision tree (BDT) algorithm [37]. For the training, simulated signal (normalization) decays are used as signal proxy, while the upper mass sideband $m(K^0_S K^0_S) > 5600$ MeV/c^2 $(m(\phi K^0_S) > 5600$ MeV/$c^2)$ in data is utilized as background proxy. To account for differences in data and simulation, the simulated decays are weighted in the B meson production kinematics and detector occupancy (represented by the number of tracks in the event) to match data distributions.

The BDT exploits the following observables: the flight distance, IP and $\chi^2_{\rm IP}$ of the B and K^0_S candidates with respect to all primary vertices, as well as the decay time, the momentum, transverse momentum and pseudorapidity of the B candidate. This set of quantities is chosen such that they have a high separation power between signal and background and are not directly correlated to the invariant mass. The same procedure is applied to the $B^0 \to \phi K^0_S$ data samples.

In order to choose the optimal threshold on the BDT response, the figure of merit $\varepsilon_{\rm sig}/(3/2 + \sqrt{N_{\rm bkg}})$ [38] is used for the signal mode, where the value $3/2$ corresponds

to a target 3 sigma significance and $\varepsilon_{\rm sig}$ is the signal efficiency of the selection, determined from simulation. The figure of merit $N_{\rm sig}/\sqrt{N_{\rm sig}+N_{\rm bkg}}$ is used for the normalization channel to minimize the uncertainty on the yield. So as not to bias the determination of the signal yield, the candidates in the signal region were not inspected until the selection was finalized. Consequently, the expected background yield $N_{\rm bkg}$ is calculated by interpolating the result of an exponential fit to data sidebands, $5000 < m(K^0_S K^0_S) < 5230$ MeV$/c^2$, and $5420 < m(K^0_S K^0_S) < 5600$ MeV$/c^2$ into the signal region. For the normalization channel, the variation of the expected signal yield $N_{\rm sig}$ as a function of the BDT response threshold is determined from simulation, while the absolute normalization is set from a single fit to the data.

The figure of merit optimization is performed simultaneously with respect to the BDT classifier output and an observable based on PID information for long track candidates, where the latter observable is corrected using a resampling from data calibration samples [39] to minimize differences in data and simulation. As a last selection step, the invariant-mass windows of $m(\pi^+\pi^-)$ and $m(K^+K^-)$ are tightened to further suppress combinatorial background. Finally, multiple candidates, which occur in about 1 in 10000 of all events, are removed randomly so that each event contains only one signal candidate.

IV. FIT STRATEGY AND RESULTS

For the normalization channel, the total $B^0 \to \phi K^0_S$ yield is obtained from extended unbinned maximum likelihood fits to the reconstructed B^0 mass in the range 5150 MeV$/c^2$ to 5600 MeV$/c^2$, separately for each data sample and reconstruction category. The signal component is modeled by a Hypatia function with power-law tails on both sides [40], where the tail parameters are fixed to values obtained from fits to simulated samples. The mean, width and signal yield parameters are free to vary in the fit. An exponential function with a free slope parameter models the combinatorial background. To account for non-ϕ contributions to the $B^0 \to \phi K^0_S$ yield, a subsequent fit is performed to the $m(K^+K^-)$ distribution, which is background-subtracted using the ${}_s\mathcal{P}$lot technique [41] and where the $m(K^+K^-K^0_S)$ distribution is used as the discriminating variable. The signal ϕ component of the $m(K^+K^-)$ fit is modeled by a relativistic Breit–Wigner function [42] convolved with a Gaussian function to take into account the resolution of the detector, while the non-ϕ contributions are described by an exponential function. The slope parameter of the latter model is Gaussian-constrained to the results obtained from fits to the simulation of $f_0(980) \to K^+K^-$ decays, which is found to better describe the observed distribution than a phase-space model. The measured yields for the normalization channel are shown in the last row of Table I. Plots of the $m(K^+K^-K^0_S)$ distributions for the Run 2 LL and LD samples are shown in Fig. 1. The remaining $m(K^+K^-K^0_S)$ distributions and the $m(K^+K^-)$ distributions are shown in the Appendix.

A Hypatia function is used to model the $m(K^0_S K^0_S)$ distribution of signal $B^0_s \to K^0_S K^0_S$ decays. All shape parameters are fixed to values obtained from fits to simulated samples. To account for resolution differences between simulation and data, the width is scaled by a factor—determined from the normalization channel—which takes values in the range 1.05 to 1.20 depending on the data sample. To model the $B^0 \to K^0_S K^0_S$ signal component, the same signal shape is duplicated and shifted by the $B^0_s - B^0$ mass difference [43]. The background component is modeled by an exponential function with a free slope parameter.

In contrast to the normalization channel, where each data category is fitted individually, a simultaneous fit to the $m(K^0_S K^0_S)$ distribution of the four data categories (Run 1 LL, Run 1 LD, Run 2 LL, Run 2 LD) is performed in the range 5000 MeV$/c^2$ to 5600 MeV$/c^2$. Two parameters are shared across all categories in the simultaneous fit, the ratio of the $B^0 \to K^0_S K^0_S$ and $B^0_s \to K^0_S K^0_S$ yields f_{B^0/B^0_s} and the branching fraction $\mathcal{B}(B^0_s \to K^0_S K^0_S)$, which is itself related to the signal yield of each data category via the relation

TABLE I. Results of the simultaneous fit to the invariant mass of the $K^0_S K^0_S$ system. The fit results for $\mathcal{B}$ and f_{B^0/B^0_s} are shared among all data categories. The given uncertainties are statistical only. The normalization constant α and the corresponding normalization channel yields $N_{\rm norm}$ are shown for reference.

Parameter	Run 1 LL	Run 1 LD	Run 2 LL	Run 2 LD	Status
$\mathcal{B}$ ($\times 10^{-6}$)		8.3 ± 1.6			Free
f_{B^0/B^0_s}		0.30 ± 0.13			Free
$N_{B^0_s}$	4.3 ± 1.0	2.1 ± 0.5	12.8 ± 2.7	12.4 ± 2.7	$\mathcal{B}/\alpha$
N_{B^0}	1.3 ± 0.5	0.63 ± 0.26	3.8 ± 1.5	3.7 ± 1.5	$f_{B^0/B^0_s} \times \mathcal{B}/\alpha$
$N_{\rm bkg}$	10.4 ± 3.5	3.5 ± 2.2	7.2 ± 3.0	13 ± 4	Free
α ($\times 10^{-6}$)	1.90 ± 0.21	3.9 ± 0.5	0.65 ± 0.05	0.66 ± 0.05	Gaussian constrained
$N_{\rm norm}$	179 ± 18	178 ± 22	316 ± 25	400 ± 31	Included in α

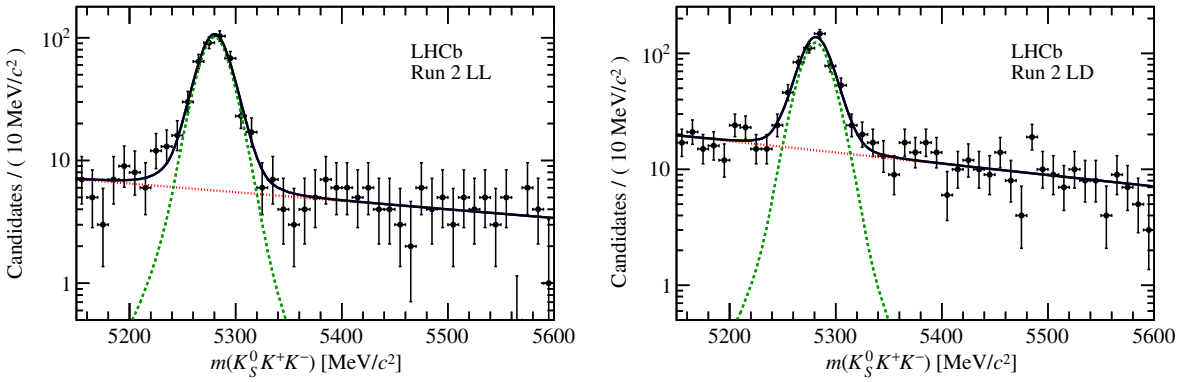

FIG. 1. Fits to the invariant-mass distribution $m(K^0_S K^+ K^-)$ of the normalization decay channel. The black curve represents the complete model, the $B^0 \to \phi K^0_S$ component is given in green (dashed), while the background component in shown in red (dotted).

$$\mathcal{B}(B^0_s \to K^0_S K^0_S) = \frac{\varepsilon_{\phi K^0_S,i}}{\varepsilon_{K^0_S K^0_S,i}} \frac{f_d}{f_s} \frac{\mathcal{B}(\phi \to K^+K^-)}{\mathcal{B}(K^0_S \to \pi^+\pi^-)} \frac{\mathcal{B}(B^0 \to \phi K^0_S)}{N_i(B^0 \to \phi K^0_S)} \cdot N_i(B^0_s \to K^0_S K^0_S)$$
$$\equiv \alpha_i \cdot N_i(B^0_s \to K^0_S K^0_S), \quad (1)$$

where the normalization constant α_i is introduced for each data category sample i. While the selection efficiencies ε and signal yields N are determined in the present analysis, external sources are used for the ratio of fragmentation fractions f_d/f_s [20,21], and the branching fractions $\mathcal{B}(B^0 \to \phi K^0_S)$, $\mathcal{B}(K^0_S \to \pi^+\pi^-)$ and $\mathcal{B}(\phi \to K^+K^-)$ [15]. To increase the robustness of the fit, the α_i constants are Gaussian constrained within their uncertainties, excluding the uncertainties from the external constants. These external uncertainties are instead applied directly to the final branching ratio measurement.

The efficiency ratio, $\varepsilon_{\phi K^0_S}/\varepsilon_{K^0_S K^0_S}$, is determined from simulation and corrected using data control samples. This ratio is found to be approximately equal to 30 in all data samples except the Run 1 LD sample, where it is twice as large due to lower trigger efficiency for downstream tracks in this sample.

The fit results are shown in Fig. 2. The results of the simultaneous mass fit are given in Table I, yielding a branching fraction of $\mathcal{B}(B^0_s \to K^0_S K^0_S) = (8.3 \pm 1.6) \times 10^{-6}$, where the uncertainty is statistical only. The $B^0_s \to K^0_S K^0_S$ yield is around 32. The ratio of the branching fractions of the signal and normalization modes $\mathcal{B}(B^0_s \to K^0_S K^0_S)/\mathcal{B}(B^0 \to \phi K^0_S)$ can also be calculated by removing the contribution of the world-average value of $\mathcal{B}(B^0 \to \phi K^0_S)$ from the fit result. This yields a combined branching fraction ratio $\mathcal{B}(B^0_s \to K^0_S K^0_S)/\mathcal{B}(B^0 \to \phi K^0_S) = 2.3 \pm 0.4$, where the uncertainty is statistical only.

From the same fit, the relative fraction of $B^0 \to K^0_S K^0_S$ decays, $f_{B^0/B^0_s} = 0.3 \pm 0.13$ is also determined. Given that the final-state particles and selections applied to the K^0_S candidates are the same for both modes, the ratio of selection efficiencies is equal to one, so that f_{B^0/B^0_s} can be converted to a ratio of branching fractions by multiplying by f_s/f_d. The calculated value of $\mathcal{B}(B^0 \to K^0_S K^0_S)/\mathcal{B}(B^0_s \to K^0_S K^0_S)$ is $(7.5 \pm 3.1) \times 10^{-2}$, where the uncertainty is statistical only.

The significances of the $B^0_s \to K^0_S K^0_S$ and $B^0 \to K^0_S K^0_S$ signal yields are estimated relative to a background-only hypothesis using Wilks' theorem [44]. The observed signal yield of 32 $B^0_s \to K^0_S K^0_S$ decays has a large significance of 8.6σ (6.5σ including the effect of systematic uncertainties), while the smaller $B^0 \to K^0_S K^0_S$ signal yield has a significance of 3.5σ including systematic uncertainties.

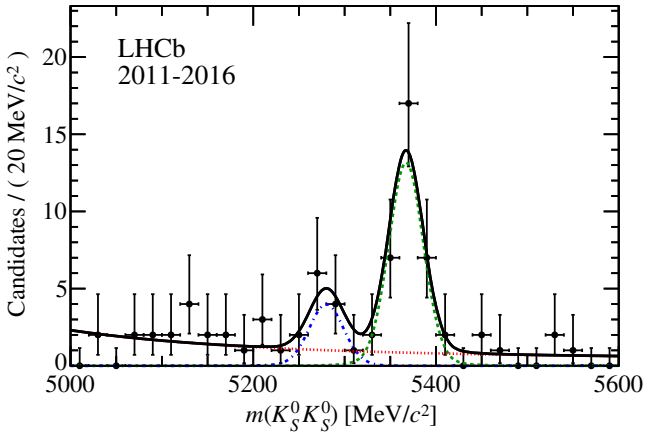

FIG. 2. Combined invariant-mass distribution $m(K^0_S K^0_S)$ of the signal decay channel. The black (solid) curve represents the complete model, the B^0_s signal component is given in green (dashed), the smaller B^0 signal is given in blue (dash-dotted) and the background component in red (dotted).

V. SYSTEMATIC UNCERTAINTIES

Each source of systematic uncertainty is evaluated independently and expressed as a relative uncertainty on the branching fraction of $B_s^0 \to K_S^0 K_S^0$ decays. A complete list is given in Table II. The uncertainties are grouped into three general categories: fit and weighting uncertainties, PID uncertainties, and detector and trigger uncertainties.

Multiple different fit uncertainties are considered. Uncertainty from possible bias in the combined fit to all four data samples can be estimated using pseudoexperiments generated and fitted according to the default fit model. In each pseudoexperiment, the number of signal candidates is drawn from a Poisson distribution with a mean determined from the baseline fit result. A relative average difference between the generated and fitted branching fraction of 5.9% is determined and conservatively assigned as a systematic uncertainty. The same procedure is performed for the $B^0 \to K_S^0 K_S^0$ component, yielding a possible bias of 1.6%. To ensure a conservative approach, the 5.9% value from $B_s^0 \to K_S^0 K_S^0$ is also applied as the systematic for $B^0 \to K_S^0 K_S^0$.

Another systematic uncertainty in the fitting process arises from the specific fit model choice, which is quantified by the use of alternative probability density functions to describe the invariant-mass distributions. The reconstructed-mass shapes for B^0 and B_s^0 mesons are modeled by the sum of two Crystal Ball functions [45]. For the fit to the $m(K^+K^-)$ distribution, the ϕ meson is modelled by a nonrelativistic Breit–Wigner function. For the normalization channel, the relative yield difference when refitting the data is taken as the systematic uncertainty, while for the $B_s^0 \to K_S^0 K_S^0$ decay pseudoexperiments are used to estimate the impact of mismodeling the shape of the signal component. The systematic uncertainty due to the choice of fit model is then the sum in quadrature of these variations, yielding values of 1.3% to 3.3% depending on the data category. Another systematic uncertainty of 2.6%, evaluated with a similar procedure, is assigned due to fixing certain shape parameters to values obtained in fits to simulated samples.

Additionally, not all differences between data and simulation can be accounted for using weights in the BDT training. As a conservative upper limit of this effect, the signal efficiency is calculated with and without weights, and the differences between these efficiencies are treated as a systematic uncertainty. This systematic uncertainty is larger by a factor of about 2 for data categories containing a downstream K_S^0 candidate than in those that contain only long K_S^0 candidates, indicating a stronger dependence of the LD channel efficiencies on the weighting.

Three sources of systematic uncertainties from PID efficiencies are considered. The effect of the finite size of the signal simulation samples is evaluated using the bootstrap method [46] for each simulation category and calculating the variance of the signal efficiency. A second systematic uncertainty is calculated by varying the model used to resample PID calibration data, and the relative difference in the signal efficiency is taken as a systematic uncertainty, though this effect is small compared to the previous source. Finally, the flight distance of the K_S^0 candidate is not considered in the resampling process, while the PID efficiency does exhibit some correlation with this variable. A systematic uncertainty is calculated by reweighting the PID distributions in bins of the K_S^0 flight distance, and calculating the relative signal efficiency on resampled simulation and resampled and reweighted simulation. The combined PID systematic uncertainty is given by summing over the three effects in quadrature, which is below 1% for the Run 1 samples and below 3% for the Run 2 samples.

Systematic uncertainties in the trigger system are divided into hardware and software trigger uncertainties. For the hardware trigger stage, the efficiency taken from simulation is compared with data calibration samples. The calibration data is used to correct the simulated efficiencies, and the

TABLE II. All systematic uncertainties on the $B_s^0 \to K_S^0 K_S^0$ branching fraction, presented as relative measurements. The last row shows the combined systematic uncertainty for each data sample.

Systematic uncertainties	Run 1, LL	Run 1, LD	Run 2, LL	Run 2, LD
Fit bias	0.059	0.059	0.059	0.059
Fit model choice	0.022	0.033	0.015	0.013
Fit model parameters	0.026	0.026	0.026	0.026
BDT	0.023	0.040	0.014	0.031
PID	0.007	0.008	0.026	0.026
Hardware trigger	0.063	0.062	0.063	0.062
Software trigger	0.065	0.106	0.008	0.026
Trigger misconfiguration	...	...	0.007	0.004
$\pi^\pm/K^\pm$ hadronic interaction	0.005	0.005	0.005	0.005
VELO misalignment	0.008	0.008	0.008	0.008
Total	0.116	0.149	0.097	0.103

resulting 6% relative difference in efficiency between the signal and normalization modes is treated as a systematic uncertainty. For the inclusive B software trigger, possible differences in efficiency between the signal and normalization channels are obtained by reweighting the $B^0 \to \phi K^0_S$ simulation to match the $B^0_s \to K^0_S K^0_S$ simulation and calculating the relative efficiency difference between the raw and reweighted distributions, yielding a systematic uncertainty of about 2%. An additional, larger systematic uncertainty is also included to account for the dedicated ϕ trigger requirements, which are only used for the normalization channel. Again, weighted $B^0 \to \phi K^0_S$ data are used to evaluate a relative efficiency difference between simulation and data, multiplied by the fraction of events solely triggered by the dedicated ϕ trigger requirements. The systematic uncertainty is about 5% to 10% in Run 1, but about 5 times smaller for Run 2. This is because the topological b-hadron trigger is more efficient in Run 2 so that there are far fewer events triggered only by the dedicated ϕ trigger. An additional systematic uncertainty less than 1% is assigned to account for a small known misconfiguration of the trigger during Run 2 data taking.

Two additional detector-related uncertainties are considered. A relative uncertainty of 0.5% is assigned due to the different hadronic interaction probabilities between pions and kaons in data and simulation, and a relative uncertainty of 0.8% is also introduced to account for a possible misalignment in the downstream positions of the vertex detector.

The combined systematic uncertainty is determined by using a weighted average of the total systematic uncertainty for each data category, where the weighting is based on the B^0_s signal yield for each category, obtained from the nominal combined fit for the branching fraction. This value is then combined with the systematic uncertainties due to the $\phi \to K^+K^-$ and $K^0_S \to \pi^+\pi^-$ branching fractions, to produce an overall systematic uncertainty of 10.7%. The systematic uncertainties due to $\mathcal{B}(B^0 \to \phi K^0_S)$ or f_s/f_d are provided separately when necessary. The total systematic uncertainty in the measurement of the B^0 branching fraction is also 10.7%.

These measurements of the branching ratio are calculated using the time-integrated event yield, without taking into account B^0_s–$\bar{B}^0_s$ mixing effects. The conversion into a branching ratio that is independent of B^0_s–$\bar{B}^0_s$ mixing can be performed according to the computation given in Ref. [47], where $\mathcal{A}^f_{\Delta\Gamma}$ is calculated from the decay amplitudes of the $B^{\rm H}_s$ and $B^{\rm L}_s$ states. In this work, the simulation is generated using the average B^0_s lifetime, corresponding to the $\mathcal{A}^f_{\Delta\Gamma} = 0$ scenario. For this scenario the mixing-corrected SM prediction of the branching ratio is equivalent to the quoted time-integrated branching ratio within uncertainties, because the impact of the scaling from $\Delta\Gamma_s/\Gamma_s = 0.135 \pm 0.008$ [15] is small.

Considering that the final state of the decay is CP -even, the relevant decay lifetime of the B^0_s is expected to be closer to that of the $B^{\rm L}_s$ state, corresponding to a SM prediction of $\mathcal{A}^f_{\Delta\Gamma}$ close to -1. This change in lifetime corresponds to a change in the expected efficiency of the $B^0_s \to K^0_S K^0_S$ reconstruction of approximately -4.5% for $\mathcal{A}^f_{\Delta\Gamma} = -1$, or $+4.5\%$ for the less-likely $\mathcal{A}^f_{\Delta\Gamma} = 1$. These scaling factors are not included in the systematic uncertainty for the time-integrated branching ratios presented below.

VI. CONCLUSION

Data collected by the LHCb experiment in 2011–2012 and 2015–2016 was used to measure the $B^0_s \to K^0_S K^0_S$ branching fraction. The measured ratio of this branching fraction relative to that of the normalization channel is

$$\frac{\mathcal{B}(B^0_s \to K^0_S K^0_S)}{\mathcal{B}(B^0 \to \phi K^0_S)} = 2.3 \pm 0.4(\text{stat}) \pm 0.2(\text{syst}) \pm 0.1(f_s/f_d),$$

where the first uncertainty is statistical, the second is systematic, and the third is due to the ratio of hadronization fractions. This is compatible with the ratio $\mathcal{B}(B^0_s \to K^0_S K^0_S)/\mathcal{B}(B^0 \to \phi K^0_S) = 2.7 \pm 0.9$ calculated from the current world average values [15].

From this measurement, the $B^0_s \to K^0_S K^0_S$ branching fraction is determined to be

$$\mathcal{B}(B^0_s \to K^0_S K^0_S) = [8.3 \pm 1.6(\text{stat}) \pm 0.9(\text{syst}) \pm 0.8(\text{norm}) \pm 0.3(f_s/f_d)] \times 10^{-6},$$

where the first uncertainty is statistical, the second is systematic, and the third and fourth are due to the normalization channel branching fraction and the ratio of hadronization fractions f_s/f_d. This result is the most precise to date and is compatible with SM predictions [6–9] and the previous measurement from the Belle collaboration [14].

In the same combined fit used for the $B^0_s \to K^0_S K^0_S$ measurement, the fraction of $B^0 \to K^0_S K^0_S$ decays is also determined. Using this measured fraction of yields, the branching fraction of $B^0 \to K^0_S K^0_S$ decays measured relative to $B^0_s \to K^0_S K^0_S$ decays is found to be

$$\frac{\mathcal{B}(B^0 \to K^0_S K^0_S)}{\mathcal{B}(B^0_s \to K^0_S K^0_S)} = [7.5 \pm 3.1(\text{stat}) \pm 0.5(\text{syst}) \pm 0.3(f_s/f_d)] \times 10^{-2},$$

where the first uncertainty is statistical, the second is systematic, and the third is due to the ratio of hadronization fractions. For comparison, calculating $\mathcal{B}(B^0 \to K^0_S K^0_S)/\mathcal{B}(B^0_s \to K^0_S K^0_S)$ based on world average-values [15] yields $(6.0 \pm 2.0)\%$, which is compatible with the obtained result.

The $B^0 \to K^0_S K^0_S$ branching fraction relative to the $B^0 \to \phi K^0_S$ normalization mode is determined to be

$$\frac{\mathcal{B}(B^0 \to K^0_S K^0_S)}{\mathcal{B}(B^0 \to \phi K^0_S)} = 0.17 \pm 0.08(\text{stat}) \pm 0.02(\text{syst}),$$

where the first uncertainty is statistical, and the second is systematic.

ACKNOWLEDGMENTS

We express our gratitude to our colleagues in the CERN accelerator departments for the excellent performance of the LHC. We thank the technical and administrative staff at the LHCb institutes. We acknowledge support from CERN and from the national agencies: CAPES, CNPq, FAPERJ and FINEP (Brazil); MOST and NSFC (China); CNRS/IN2P3 (France); BMBF, DFG and MPG (Germany); INFN (Italy); NWO (Netherlands); MNiSW and NCN (Poland); MEN/IFA (Romania); MSHE (Russia); MinECo (Spain); SNSF and SER (Switzerland); NASU (Ukraine); STFC (United Kingdom); DOE NP and NSF (USA). We acknowledge the computing resources that are provided by CERN, IN2P3 (France), KIT and DESY (Germany), INFN (Italy), SURF (Netherlands), PIC (Spain), GridPP (United Kingdom), RRCKI and Yandex LLC (Russia), CSCS (Switzerland), IFIN-HH (Romania), CBPF (Brazil), PL-GRID (Poland) and OSC (USA). We are indebted to the communities behind the multiple open-source software packages on which we depend. Individual groups or members have received support from AvH Foundation (Germany); EPLANET, Marie Skłodowska-Curie Actions and ERC (European Union); ANR, Labex P2IO and OCEVU, and Région Auvergne-Rhône-Alpes (France); Key Research Program of Frontier Sciences of CAS, CAS PIFI, and the Thousand Talents Program (China); RFBR, RSF and Yandex LLC (Russia); GVA, XuntaGal and GENCAT (Spain); the Royal Society and the Leverhulme Trust (United Kingdom).

APPENDIX: NORMALIZATION CHANNEL FITS

Figure 3 shows the $m(K^+K^-K^0_S)$ distributions for the Run 1 LL and LD categories. The $m(K+K-)$ distributions for all four data categories are shown in Fig. 4.

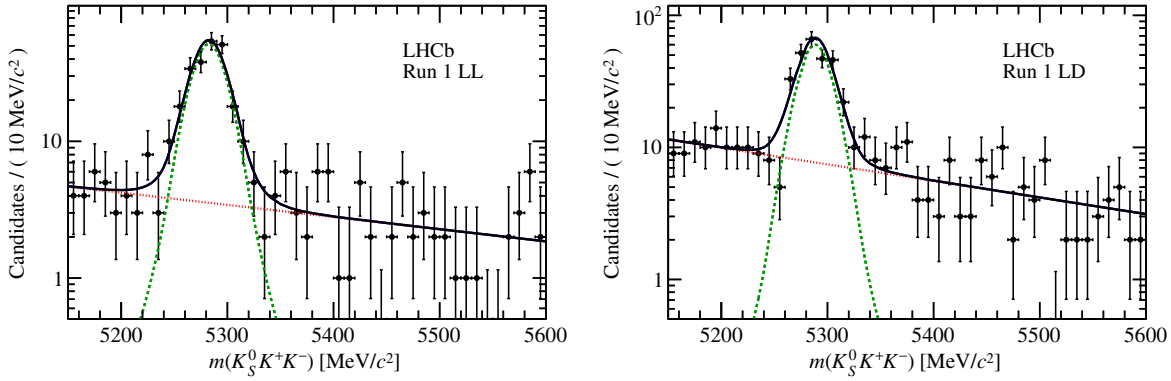

FIG. 3. Fits to the invariant-mass distribution $m(K^0_S K^+K^-)$ of the normalization decay channel. The black curve represents the complete model, the $B^0 \to \phi K^0_S$ component is given in green (dashed), while the background component in shown in red (dotted).

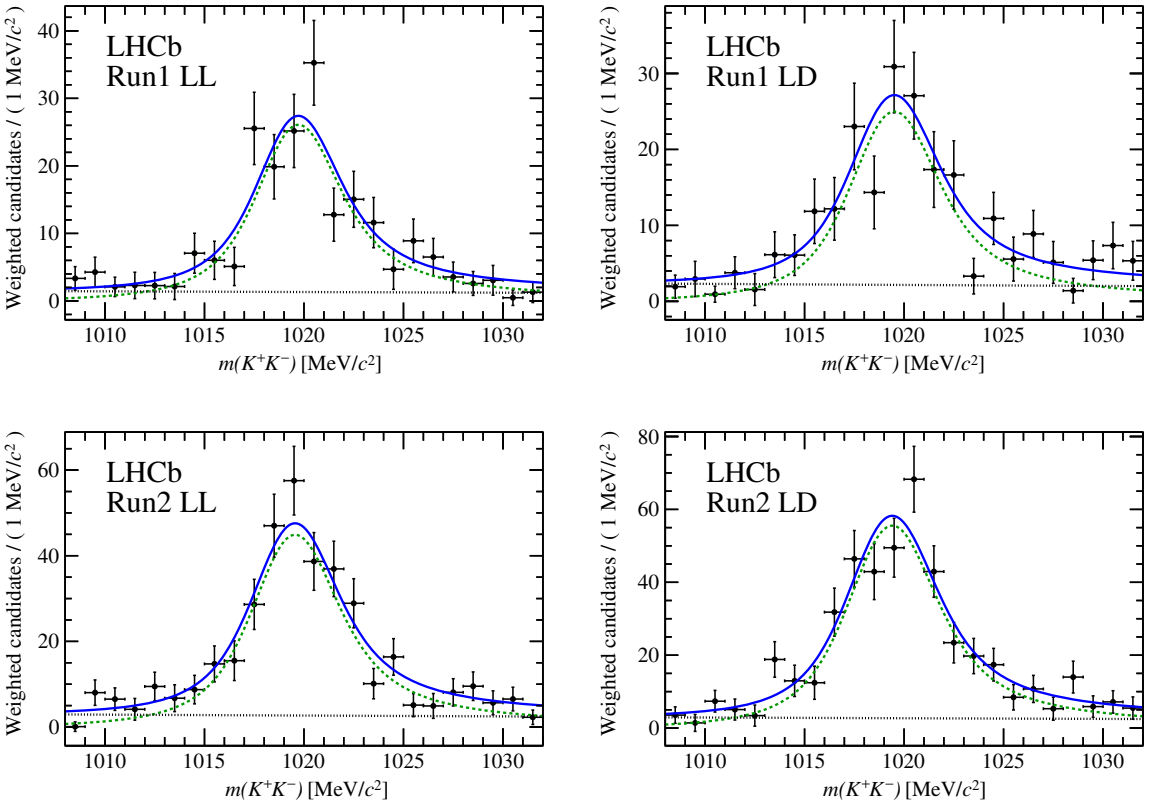

FIG. 4. Fits to the invariant-mass distribution $m(K^+K^-)$ of $B^0 \to \phi K^0_S$ data weighted using the ${}_s\mathcal{P}$lot technique. The blue curve represents the complete model, the signal ϕ component is given in green (dashed), and the background $f_0(980) \to K^+K^-$ model is shown in black (dotted).

[1] R. Aaij *et al.* (LHCb Collaboration), Amplitude analysis of the $B^0_{(s)} \to K^{*0}\bar{K}^{*0}$ decays and measurement of the branching fraction of the $B^0 \to K^{*0}\bar{K}^{*0}$ decay, J. High Energy Phys. 07 (2019) 032.

[2] R. Aaij *et al.* (LHCb Collaboration), First measurement of the *CP*-violating phase $\phi_s^{d\bar{d}}$ in $B^0_s \to (K^+\pi^-)(K^-\pi^+)$ decays, J. High Energy Phys. 03 (2018) 140.

[3] R. Aaij *et al.* (LHCb Collaboration), Amplitude analysis of $B^0_s \to K^0_S K^\pm \pi^\mp$ decays, J. High Energy Phys. 06 (2019) 114.

[4] R. Aaij *et al.* (LHCb Collaboration), Observation of the Annihilation Decay Mode $B^0 \to K^+K^-$, Phys. Rev. Lett. **118**, 081801 (2017).

[5] S. Baek, D. London, J. Matias, and J. Virto, $B^0_s \to K^+K^-$ and $B^0_s \to K^0\bar{K}^0$ decays within supersymmetry, J. High Energy Phys. 12 (2006) 019.

[6] A. R. Williamson and J. Zupan, Two body B decays with isosinglet final states in SCET, Phys. Rev. D **74**, 014003 (2006); Erratum, Phys. Rev. D **74**, 03901 (2017).

[7] M. Beneke and M. Neubert, QCD factorization for $B^0_{(s)} \to PP$ and $B^0_{(s)} \to PV$ decays, Nucl. Phys. **B675**, 333 (2003).

[8] A. Ali, G. Kramer, Y. Li, C.-D. Lü, Y.-L. Shen, W. Wang, and Y.-M. Wang, Charmless nonleptonic B_s decays to PP, PV, and VV final states in the perturbative QCD approach, Phys. Rev. D **76**, 074018 (2007).

[9] J.-J. Wang, D.-T. Lin, W. Sun, Z.-J. Ji, S. Cheng, and Z.-J. Xiao, $B^0_s \to K\pi, KK$ decays and effects of the next-to-leading order contributions, Phys. Rev. D **89**, 074046 (2014).

[10] Q. Chang, X.-Q. Li, and Y.-D. Yang, A comprehensive analysis of hadronic $b \to s$ transitions in a family non-universal Z' model, J. Phys. G **41**, 105002 (2014).

[11] S. Descotes-Genon, J. Matias, and J. Virto, Exploring $B^0_s \to KK$ Decays Through Flavour Symmetries and QCD-Factorisation, Phys. Rev. Lett. **97**, 061801 (2006).

[12] M. Ciuchini, M. Pierini, and L. Silvestrini, $B^0_s \to K^{(*)0}\bar{K}^{(*)0}$ Decays: The Golden Channels for New Physics Searches, Phys. Rev. Lett. **100**, 031802 (2008).

[13] B. Bhattacharya, A. Datta, M. Imbeault, and D. London, Measuring β_s with $B_s \to K^{0(*)}\bar{K}^{*0}$–a reappraisal, Phys. Lett. B **717**, 403 (2012).

[14] B. Pal *et al.* (Belle Collaboration), Observation of the Decay $B^0_s \to K^0\bar{K}^0$, Phys. Rev. Lett. **116**, 161801 (2016).

[15] M. Tanabashi *et al.* (Particle Data Group), Review of particle physics, Phys. Rev. D **98**, 030001 (2018).

[16] Y.-T. Duh *et al.* (Belle Collaboration), Measurements of branching fractions and direct CP asymmetries for $B \to K\pi$, $B \to \pi\pi$ and $B \to KK$ decays, Phys. Rev. D **87**, 031103 (2013).

[17] B. Aubert *et al.* (*BABAR* Collaboration), Observation of $B^+ \to \bar{K}^0 K^+$ and $B^0 \to K^0 \bar{K}^0$, Phys. Rev. Lett. **97**, 171805 (2006).

[18] J. P. Lees *et al.* (*BABAR* Collaboration), Study of CP violation in Dalitz-plot analyses of $B^0 \to K^+K^-K^0_S$, $B^+ \to K^+K^-K^+$ and $B^+ \to K^0_S K^0_S K^+$, Phys. Rev. D **85**, 112010 (2012).

[19] K. F. Chen *et al.* (Belle Collaboration), Measurement of Branching Fractions and Polarization in $B \to \phi K^{(*)}$ Decays, Phys. Rev. Lett. **91**, 201801 (2003).

[20] R. Aaij *et al.* (LHCb Collaboration), Measurement of the fragmentation fraction ratio f_s/f_d and its dependence on B meson kinematics, J. High Energy Phys. 04 (2013) 001, f_s/f_d value updated in LHCb-CONF-2013-011.

[21] R. Aaij *et al.* (LHCb Collaboration), Measurement of b-hadron fractions in 13 TeV pp collisions, Phys. Rev. D **100**, 031102(R) (2019).

[22] A. A. Alves Jr. *et al.* (LHCb Collaboration), The LHCb detector at the LHC, J. Instrum. **3**, S08005 (2008).

[23] R. Aaij *et al.* (LHCb Collaboration), LHCb detector performance, Int. J. Mod. Phys. A **30**, 1530022 (2015).

[24] R. Aaij *et al.*, Performance of the LHCb vertex locator, J. Instrum. **9**, P09007 (2014).

[25] R. Arink *et al.*, Performance of the LHCb outer tracker, J. Instrum. **9**, P01002 (2014).

[26] P. d'Argent *et al.*, Improved performance of the LHCb outer tracker in LHC Run 2, J. Instrum. **12**, P11016 (2017).

[27] M. Adinolfi *et al.*, Performance of the LHCb RICH detector at the LHC, Eur. Phys. J. C **73**, 2431 (2013).

[28] R. Aaij *et al.*, The LHCb trigger and its performance in 2011, J. Instrum. **8**, P04022 (2013).

[29] V. V. Gligorov and M. Williams, Efficient, reliable and fast high-level triggering using a bonsai boosted decision tree, J. Instrum. **8**, P02013 (2013).

[30] T. Sjöstrand, S. Mrenna, and P. Skands, PYTHIA 6.4 physics and manual, J. High Energy Phys. 05 (2006) 026; A brief introduction to PYTHIA 8.1, Comput. Phys. Commun. **178**, 852 (2008).

[31] I. Belyaev *et al.*, Handling of the generation of primary events in Gauss, the LHCb simulation framework, J. Phys. Conf. Ser. **331**, 032047 (2011).

[32] D. J. Lange, The EvtGen particle decay simulation package, Nucl. Instrum. Methods Phys. Res., Sect. A **462**, 152 (2001).

[33] P. Golonka and Z. Was, PHOTOS Monte Carlo: A precision tool for QED corrections in Z and W decays, Eur. Phys. J. C **45**, 97 (2006).

[34] J. Allison *et al.* (Geant4 Collaboration), GEANT4 developments and applications, IEEE Trans. Nucl. Sci. **53**, 270 (2006); S. Agostinelli *et al.* (Geant4 Collaboration), GEANT4: A simulation toolkit, Nucl. Instrum. Methods Phys. Res., Sect. A **506**, 250 (2003).

[35] M. Clemencic *et al.* (LHCB Collaboration), The LHCb simulation application, Gauss: Design, evolution and experience, J. Phys. Conf. Ser. **331**, 032023 (2011).

[36] T. Chen and C. Guestrin, XGBoost: A scalable tree boosting system, *KDD '16: Proceedings of the 22nd ACM SIGKDD International Conference on Knowledge Discovery and Data MiningAugust* (ACM Digital Library, 2016), p. 785.

[37] L. Breiman, J. H. Friedman, R. A. Olshen, and C. J. Stone, *Classification and Regression Trees* (Wadsworth International Group, Belmont, CA, 1984).

[38] G. Punzi, Sensitivity of searches for new signals and its optimization, eConf **C030908**, MODT002 (2003), https://inspirehep.net/literature/634798.

[39] R. Aaij *et al.*, Selection and processing of calibration samples to measure the particle identification performance of the LHCb experiment in Run 2, Eur. Phys. J. Tech. Instrum. **6**, 1 (2018).

[40] D. Martínez Santos and F. Dupertuis, Mass distributions marginalized over per-event errors, Nucl. Instrum. Methods Phys. Res., Sect. A **764**, 150 (2014).

[41] M. Pivk and F. R. Le Diberder, sPlot: A statistical tool to unfold data distributions, Nucl. Instrum. Methods Phys. Res., Sect. A **555**, 356 (2005).

[42] R. A. Kycia and S. Jadach, Relativistic Voigt profile for unstable particles in high energy physics, J. Math. Anal. Appl. **463**, 1040 (2018).

[43] R. Aaij *et al.* (LHCb Collaboration), Observation of the decay $\bar{B}^0_s \to \psi(2S)K^+\pi^-$, Phys. Lett. B **747**, 484 (2015).

[44] S. S. Wilks, The large-sample distribution of the likelihood ratio for testing composite hypotheses, Ann. Math. Stat. **9**, 60 (1938).

[45] T. Skwarnicki, A study of the radiative cascade transitions between the Upsilon-prime and Upsilon resonances, Ph.D. thesis, Institute of Nuclear Physics, 1986, DESY-F31-86-02.

[46] B. Efron and R. J. Tibshirani, *An Introduction to the Bootstrap*, Mono. Stat. Appl. Probab. (Chapman and Hall, London, 1993).

[47] K. De Bruyn, R. Fleischer, R. Knegjens, P. Koppenburg, M. Merk, and N. Tuning, Branching ratio measurements of B_s decays, Phys. Rev. D **86**, 014027 (2012).

R. Aaij,[31] C. Abellán Beteta,[49] T. Ackernley,[59] B. Adeva,[45] M. Adinolfi,[53] H. Afsharnia,[9] C. A. Aidala,[79] S. Aiola,[25] Z. Ajaltouni,[9] S. Akar,[64] P. Albicocco,[22] J. Albrecht,[14] F. Alessio,[47] M. Alexander,[58] A. Alfonso Albero,[44] G. Alkhazov,[37] P. Alvarez Cartelle,[60] A. A. Alves Jr.,[45] S. Amato,[2] Y. Amhis,[11] L. An,[21] L. Anderlini,[21] G. Andreassi,[48] M. Andreotti,[20] F. Archilli,[16] J. Arnau Romeu,[10] A. Artamonov,[43] M. Artuso,[67] K. Arzymatov,[41] E. Aslanides,[10] M. Atzeni,[49] B. Audurier,[26] S. Bachmann,[16] J. J. Back,[55] S. Baker,[60] V. Balagura,[11,b] W. Baldini,[20,47] A. Baranov,[41] R. J. Barlow,[61] S. Barsuk,[11] W. Barter,[60] M. Bartolini,[23,47,c] F. Baryshnikov,[76] G. Bassi,[28] V. Batozskaya,[35] B. Batsukh,[67] A. Battig,[14] V. Battista,[48]

A. Bay,[48] M. Becker,[14] F. Bedeschi,[28] I. Bediaga,[1] A. Beiter,[67] L. J. Bel,[31] V. Belavin,[41] S. Belin,[26] N. Beliy,[5] V. Bellee,[48] K. Belous,[43] I. Belyaev,[38] G. Bencivenni,[22] E. Ben-Haim,[12] S. Benson,[31] S. Beranek,[13] A. Berezhnoy,[39] R. Bernet,[49] D. Berninghoff,[16] H. C. Bernstein,[67] E. Bertholet,[12] A. Bertolin,[27] C. Betancourt,[49] F. Betti,[19,d] M. O. Bettler,[54] Ia. Bezshyiko,[49] S. Bhasin,[53] J. Bhom,[33] M. S. Bieker,[14] S. Bifani,[52] P. Billoir,[12] A. Bizzeti,[21,e] M. Bjørn,[62] M. P. Blago,[47] T. Blake,[55] F. Blanc,[48] S. Blusk,[67] D. Bobulska,[58] V. Bocci,[30] O. Boente Garcia,[45] T. Boettcher,[63] A. Boldyrev,[77] A. Bondar,[42,f] N. Bondar,[37] S. Borghi,[61,47] M. Borisyak,[41] M. Borsato,[16] J. T. Borsuk,[33] T. J. V. Bowcock,[59] C. Bozzi,[20] S. Braun,[16] A. Brea Rodriguez,[45] M. Brodski,[47] J. Brodzicka,[33] A. Brossa Gonzalo,[55] D. Brundu,[26] E. Buchanan,[53] A. Büchler-Germann,[49] A. Buonaura,[49] C. Burr,[47] A. Bursche,[26] J. S. Butter,[31] J. Buytaert,[47] W. Byczynski,[47] S. Cadeddu,[26] H. Cai,[71] R. Calabrese,[20,g] S. Cali,[22] R. Calladine,[52] M. Calvi,[24,h] M. Calvo Gomez,[44,i] A. Camboni,[44,i] P. Campana,[22] D. H. Campora Perez,[47] L. Capriotti,[19,d] A. Carbone,[19,d] G. Carboni,[29] R. Cardinale,[23,c] A. Cardini,[26] P. Carniti,[24,h] K. Carvalho Akiba,[31] A. Casais Vidal,[45] G. Casse,[59] M. Cattaneo,[47] G. Cavallero,[47] R. Cenci,[28,j] J. Cerasoli,[10] M. G. Chapman,[53] M. Charles,[12,47] Ph. Charpentier,[47] G. Chatzikonstantinidis,[52] M. Chefdeville,[8] V. Chekalina,[41] C. Chen,[3] S. Chen,[26] A. Chernov,[33] S.-G. Chitic,[47] V. Chobanova,[45] M. Chrzaszcz,[47] A. Chubykin,[37] P. Ciambrone,[22] M. F. Cicala,[55] X. Cid Vidal,[45] G. Ciezarek,[47] F. Cindolo,[19] P. E. L. Clarke,[57] M. Clemencic,[47] H. V. Cliff,[54] J. Closier,[47] J. L. Cobbledick,[61] V. Coco,[47] J. A. B. Coelho,[11] J. Cogan,[10] E. Cogneras,[9] L. Cojocariu,[36] P. Collins,[47] T. Colombo,[47] A. Comerma-Montells,[16] A. Contu,[26] N. Cooke,[52] G. Coombs,[58] S. Coquereau,[44] G. Corti,[47] C. M. Costa Sobral,[55] B. Couturier,[47] D. C. Craik,[63] J. Crkovská,[66] A. Crocombe,[55] M. Cruz Torres,[1,k] R. Currie,[57] C. L. Da Silva,[66] E. Dall'Occo,[31] J. Dalseno,[45,53] C. D'Ambrosio,[47] A. Danilina,[38] P. d'Argent,[16] A. Davis,[61] O. De Aguiar Francisco,[47] K. De Bruyn,[47] S. De Capua,[61] M. De Cian,[48] J. M. De Miranda,[1] L. De Paula,[2] M. De Serio,[18,l] P. De Simone,[22] J. A. de Vries,[31] C. T. Dean,[66] W. Dean,[79] D. Decamp,[8] L. Del Buono,[12] B. Delaney,[54] H.-P. Dembinski,[15] M. Demmer,[14] A. Dendek,[34] V. Denysenko,[49] D. Derkach,[77] O. Deschamps,[9] F. Desse,[11] F. Dettori,[26,m] B. Dey,[7] A. Di Canto,[47] P. Di Nezza,[22] S. Didenko,[76] H. Dijkstra,[47] F. Dordei,[26] M. Dorigo,[28,n] A. C. dos Reis,[1] L. Douglas,[58] A. Dovbnya,[50] K. Dreimanis,[59] M. W. Dudek,[33] L. Dufour,[47] G. Dujany,[12] P. Durante,[47] J. M. Durham,[66] D. Dutta,[61] R. Dzhelyadin,[43,a] M. Dziewiecki,[16] A. Dziurda,[33] A. Dzyuba,[37] S. Easo,[56] U. Egede,[60] V. Egorychev,[38] S. Eidelman,[42,f] S. Eisenhardt,[57] R. Ekelhof,[14] S. Ek-In,[48] L. Eklund,[58] S. Ely,[67] A. Ene,[36] S. Escher,[13] S. Esen,[31] T. Evans,[47] A. Falabella,[19] J. Fan,[3] N. Farley,[52] S. Farry,[59] D. Fazzini,[11] M. Féo,[47] P. Fernandez Declara,[47] A. Fernandez Prieto,[45] F. Ferrari,[19,d] L. Ferreira Lopes,[48] F. Ferreira Rodrigues,[2] S. Ferreres Sole,[31] M. Ferrillo,[49] M. Ferro-Luzzi,[47] S. Filippov,[40] R. A. Fini,[18] M. Fiorini,[20,g] M. Firlej,[34] K. M. Fischer,[62] C. Fitzpatrick,[47] T. Fiutowski,[34] F. Fleuret,[11,b] M. Fontana,[47] F. Fontanelli,[23,c] R. Forty,[47] V. Franco Lima,[59] M. Franco Sevilla,[65] M. Frank,[47] C. Frei,[47] D. A. Friday,[58] J. Fu,[25,o] Q. Fuehring,[14] W. Funk,[47] E. Gabriel,[57] A. Gallas Torreira,[45] D. Galli,[19,d] S. Gallorini,[27] S. Gambetta,[57] Y. Gan,[3] M. Gandelman,[2] P. Gandini,[25] Y. Gao,[4] L. M. Garcia Martin,[46] J. García Pardiñas,[49] B. Garcia Plana,[45] F. A. Garcia Rosales,[11] J. Garra Tico,[54] L. Garrido,[44] D. Gascon,[44] C. Gaspar,[47] D. Gerick,[16] E. Gersabeck,[61] M. Gersabeck,[61] T. Gershon,[55] D. Gerstel,[10] Ph. Ghez,[8] V. Gibson,[54] A. Gioventù,[45] O. G. Girard,[48] P. Gironella Gironell,[44] L. Giubega,[36] C. Giugliano,[20] K. Gizdov,[57] V. V. Gligorov,[12] C. Göbel,[69] E. Golobardes,[44,i] D. Golubkov,[38] A. Golutvin,[60,76] A. Gomes,[1,p] P. Gorbounov,[38,6] I. V. Gorelov,[39] C. Gotti,[24,h] E. Govorkova,[31] J. P. Grabowski,[16] R. Graciani Diaz,[44] T. Grammatico,[12] L. A. Granado Cardoso,[47] E. Graugés,[44] E. Graverini,[48] G. Graziani,[21] A. Grecu,[36] R. Greim,[31] P. Griffith,[20] L. Grillo,[61] L. Gruber,[47] B. R. Gruberg Cazon,[62] C. Gu,[3] E. Gushchin,[40] A. Guth,[13] Yu. Guz,[43,47] T. Gys,[47] T. Hadavizadeh,[62] G. Haefeli,[48] C. Haen,[47] S. C. Haines,[54] P. M. Hamilton,[65] Q. Han,[7] X. Han,[16] T. H. Hancock,[62] S. Hansmann-Menzemer,[16] N. Harnew,[62] T. Harrison,[59] R. Hart,[31] C. Hasse,[47] M. Hatch,[47] J. He,[5] M. Hecker,[60] K. Heijhoff,[31] K. Heinicke,[14] A. Heister,[14] A. M. Hennequin,[47] K. Hennessy,[59] L. Henry,[46] J. Heuel,[13] A. Hicheur,[68] R. Hidalgo Charman,[61] D. Hill,[62] M. Hilton,[61] S. Hollitt,[14] P. H. Hopchev,[48] J. Hu,[16] W. Hu,[7] W. Huang,[5] Z. C. Huard,[64] W. Hulsbergen,[31] T. Humair,[60] R. J. Hunter,[55] M. Hushchyn,[77] D. Hutchcroft,[59] D. Hynds,[31] P. Ibis,[14] M. Idzik,[34] P. Ilten,[52] A. Inglessi,[37] A. Inyakin,[43] K. Ivshin,[37] R. Jacobsson,[47] S. Jakobsen,[47] J. Jalocha,[62] E. Jans,[31] B. K. Jashal,[46] A. Jawahery,[65] V. Jevtic,[14] F. Jiang,[3] M. John,[62] D. Johnson,[47] C. R. Jones,[54] B. Jost,[47] N. Jurik,[62] S. Kandybei,[50] M. Karacson,[47] J. M. Kariuki,[53] N. Kazeev,[77] M. Kecke,[16] F. Keizer,[54] M. Kelsey,[67] M. Kenzie,[54] T. Ketel,[32] B. Khanji,[47] A. Kharisova,[78] K. E. Kim,[67] T. Kirn,[13] V. S. Kirsebom,[48] S. Klaver,[22] K. Klimaszewski,[35] S. Koliiev,[51] A. Kondybayeva,[76] A. Konoplyannikov,[38] P. Kopciewicz,[34] R. Kopecna,[16] P. Koppenburg,[31] M. Korolev,[39] I. Kostiuk,[31,51] O. Kot,[51] S. Kotriakhova,[37] L. Kravchuk,[40] R. D. Krawczyk,[47] M. Kreps,[55] F. Kress,[60] S. Kretzschmar,[13] P. Krokovny,[42,f] W. Krupa,[34] W. Krzemien,[35] W. Kucewicz,[33,q] M. Kucharczyk,[33] V. Kudryavtsev,[42,f] H. S. Kuindersma,[31] G. J. Kunde,[66] A. K. Kuonen,[48] T. Kvaratskheliya,[38] D. Lacarrere,[47] G. Lafferty,[61] A. Lai,[26] D. Lancierini,[49] J. J. Lane,[61] G. Lanfranchi,[22]

C. Langenbruch,[13] T. Latham,[55] F. Lazzari,[28,r] C. Lazzeroni,[52] R. Le Gac,[10] R. Lefèvre,[9] A. Leflat,[39] F. Lemaitre,[47] O. Leroy,[10] T. Lesiak,[33] B. Leverington,[16] H. Li,[70] X. Li,[66] Y. Li,[6] Z. Li,[67] X. Liang,[67] R. Lindner,[47] F. Lionetto,[49] V. Lisovskyi,[11] G. Liu,[70] X. Liu,[3] D. Loh,[55] A. Loi,[26] J. Lomba Castro,[45] I. Longstaff,[58] J. H. Lopes,[2] G. Loustau,[49] G. H. Lovell,[54] Y. Lu,[6] D. Lucchesi,[27,s] M. Lucio Martinez,[31] Y. Luo,[3] A. Lupato,[27] E. Luppi,[20,g] O. Lupton,[55] A. Lusiani,[28,t] X. Lyu,[5] S. Maccolini,[19,d] F. Machefert,[11] F. Maciuc,[36] V. Macko,[48] P. Mackowiak,[14] S. Maddrell-Mander,[53] L. R. Madhan Mohan,[53] O. Maev,[37,47] A. Maevskiy,[77] K. Maguire,[61] D. Maisuzenko,[37] M. W. Majewski,[34] S. Malde,[62] B. Malecki,[47] A. Malinin,[75] T. Maltsev,[42,f] H. Malygina,[16] G. Manca,[26,m] G. Mancinelli,[10] R. Manera Escalero,[44] D. Manuzzi,[19,d] D. Marangotto,[25,o] J. Maratas,[9,u] J. F. Marchand,[8] U. Marconi,[19] S. Mariani,[21] C. Marin Benito,[11] M. Marinangeli,[48] P. Marino,[48] J. Marks,[16] P. J. Marshall,[59] G. Martellotti,[30] L. Martinazzoli,[47] M. Martinelli,[24,h] D. Martinez Santos,[45] F. Martinez Vidal,[46] A. Massafferri,[1] M. Materok,[13] R. Matev,[47] A. Mathad,[49] Z. Mathe,[47] V. Matiunin,[38] C. Matteuzzi,[24] K. R. Mattioli,[79] A. Mauri,[49] E. Maurice,[11,b] M. McCann,[60,47] L. Mcconnell,[17] A. McNab,[61] R. McNulty,[17] J. V. Mead,[59] B. Meadows,[64] C. Meaux,[10] G. Meier,[14] N. Meinert,[73] D. Melnychuk,[35] S. Meloni,[24,h] M. Merk,[31] A. Merli,[25] M. Mikhasenko,[47] D. A. Milanes,[72] E. Millard,[55] M.-N. Minard,[8] O. Mineev,[38] L. Minzoni,[20,g] S. E. Mitchell,[57] B. Mitreska,[61] D. S. Mitzel,[47] A. Mödden,[14] A. Mogini,[12] R. D. Moise,[60] T. Mombächer,[14] I. A. Monroy,[72] S. Monteil,[9] M. Morandin,[27] G. Morello,[22] M. J. Morello,[28,t] J. Moron,[34] A. B. Morris,[10] A. G. Morris,[55] R. Mountain,[67] H. Mu,[3] F. Muheim,[57] M. Mukherjee,[7] M. Mulder,[31] D. Müller,[47] K. Müller,[49] V. Müller,[14] C. H. Murphy,[62] D. Murray,[61] P. Muzzetto,[26] P. Naik,[53] T. Nakada,[48] R. Nandakumar,[56] A. Nandi,[62] T. Nanut,[48] I. Nasteva,[2] M. Needham,[57] N. Neri,[25,o] S. Neubert,[16] N. Neufeld,[47] R. Newcombe,[60] T. D. Nguyen,[48] C. Nguyen-Mau,[48,v] E. M. Niel,[11] S. Nieswand,[13] N. Nikitin,[39] N. S. Nolte,[47] A. Oblakowska-Mucha,[34] V. Obraztsov,[43] S. Ogilvy,[58] D. P. O'Hanlon,[19] R. Oldeman,[26,m] C. J. G. Onderwater,[74] J. D. Osborn,[79] A. Ossowska,[33] J. M. Otalora Goicochea,[2] T. Ovsiannikova,[38] P. Owen,[49] A. Oyanguren,[46] P. R. Pais,[48] T. Pajero,[28,t] A. Palano,[18] M. Palutan,[22] G. Panshin,[78] A. Papanestis,[56] M. Pappagallo,[57] L. L. Pappalardo,[20,g] W. Parker,[65] C. Parkes,[61,47] G. Passaleva,[21,47] A. Pastore,[18] M. Patel,[60] C. Patrignani,[19,d] A. Pearce,[47] A. Pellegrino,[31] M. Pepe Altarelli,[47] S. Perazzini,[19] D. Pereima,[38] P. Perret,[9] L. Pescatore,[48] K. Petridis,[53] A. Petrolini,[23,c] A. Petrov,[75] S. Petrucci,[57] M. Petruzzo,[25,o] B. Pietrzyk,[8] G. Pietrzyk,[48] M. Pikies,[33] M. Pili,[62] D. Pinci,[30] J. Pinzino,[47] F. Pisani,[47] A. Piucci,[16] V. Placinta,[36] S. Playfer,[57] J. Plews,[52] M. Plo Casasus,[45] F. Polci,[12] M. Poli Lener,[22] M. Poliakova,[67] A. Poluektov,[10] N. Polukhina,[76,w] I. Polyakov,[67] E. Polycarpo,[2] G. J. Pomery,[53] S. Ponce,[47] A. Popov,[43] D. Popov,[52] S. Poslavskii,[43] K. Prasanth,[33] L. Promberger,[47] C. Prouve,[45] V. Pugatch,[51] A. Puig Navarro,[49] H. Pullen,[62] G. Punzi,[28,j] W. Qian,[5] J. Qin,[5] R. Quagliani,[12] B. Quintana,[9] N. V. Raab,[17] R. I. Rabadan Trejo,[10] B. Rachwal,[34] J. H. Rademacker,[53] M. Rama,[28] M. Ramos Pernas,[45] M. S. Rangel,[2] F. Ratnikov,[41,77] G. Raven,[32] M. Ravonel Salzgeber,[47] M. Reboud,[8] F. Redi,[48] S. Reichert,[14] F. Reiss,[12] C. Remon Alepuz,[46] Z. Ren,[3] V. Renaudin,[62] S. Ricciardi,[56] S. Richards,[53] K. Rinnert,[59] P. Robbe,[11] A. Robert,[12] A. B. Rodrigues,[48] E. Rodrigues,[64] J. A. Rodriguez Lopez,[72] M. Roehrken,[47] S. Roiser,[47] A. Rollings,[62] V. Romanovskiy,[43] M. Romero Lamas,[45] A. Romero Vidal,[45] J. D. Roth,[79] M. Rotondo,[22] M. S. Rudolph,[67] T. Ruf,[47] J. Ruiz Vidal,[46] J. Ryzka,[34] J. J. Saborido Silva,[45] N. Sagidova,[37] B. Saitta,[26,m] C. Sanchez Gras,[31] C. Sanchez Mayordomo,[46] B. Sanmartin Sedes,[45] R. Santacesaria,[30] C. Santamarina Rios,[45] M. Santimaria,[22] E. Santovetti,[29,x] G. Sarpis,[61] A. Sarti,[30] C. Satriano,[30,y] A. Satta,[29] M. Saur,[5] D. Savrina,[38,39] L. G. Scantlebury Smead,[62] S. Schael,[13] M. Schellenberg,[14] M. Schiller,[58] H. Schindler,[47] M. Schmelling,[15] T. Schmelzer,[14] B. Schmidt,[47] O. Schneider,[48] A. Schopper,[47] H. F. Schreiner,[64] M. Schubiger,[31] S. Schulte,[48] M. H. Schune,[11] R. Schwemmer,[47] B. Sciascia,[22] A. Sciubba,[30,z] S. Sellam,[68] A. Semennikov,[38] A. Sergi,[52,47] N. Serra,[49] J. Serrano,[10] L. Sestini,[27] A. Seuthe,[14] P. Seyfert,[47] D. M. Shangase,[79] M. Shapkin,[43] T. Shears,[59] L. Shekhtman,[42,f] V. Shevchenko,[75,76] E. Shmanin,[76] J. D. Shupperd,[67] B. G. Siddi,[20] R. Silva Coutinho,[49] L. Silva de Oliveira,[2] G. Simi,[27,s] S. Simone,[18,l] I. Skiba,[20] N. Skidmore,[16] T. Skwarnicki,[67] M. W. Slater,[52] J. G. Smeaton,[54] A. Smetkina,[38] E. Smith,[13] I. T. Smith,[57] M. Smith,[60] A. Snoch,[31] M. Soares,[19] L. Soares Lavra,[1] M. D. Sokoloff,[64] F. J. P. Soler,[58] B. Souza De Paula,[2] B. Spaan,[14] E. Spadaro Norella,[25,o] P. Spradlin,[58] F. Stagni,[47] M. Stahl,[64] S. Stahl,[47] P. Stefko,[48] S. Stefkova,[60] O. Steinkamp,[49] S. Stemmle,[16] O. Stenyakin,[43] M. Stepanova,[37] H. Stevens,[14] S. Stone,[67] S. Stracka,[28] M. E. Stramaglia,[48] M. Straticiuc,[36] S. Strokov,[78] J. Sun,[3] L. Sun,[71] Y. Sun,[65] P. Svihra,[61] K. Swientek,[34] A. Szabelski,[35] T. Szumlak,[34] M. Szymanski,[5] S. Taneja,[61] Z. Tang,[3] T. Tekampe,[14] G. Tellarini,[20] F. Teubert,[47] E. Thomas,[47] K. A. Thomson,[59] M. J. Tilley,[60] V. Tisserand,[9] S. T'Jampens,[8] M. Tobin,[6] S. Tolk,[47] L. Tomassetti,[20,g] D. Tonelli,[28] D. Y. Tou,[12] E. Tournefier,[8] M. Traill,[58] M. T. Tran,[48] A. Trisovic,[54] A. Tsaregorodtsev,[10] G. Tuci,[28,47,j] A. Tully,[48] N. Tuning,[31] A. Ukleja,[35] A. Usachov,[11] A. Ustyuzhanin,[41,77] U. Uwer,[16] A. Vagner,[78] V. Vagnoni,[19] A. Valassi,[47] G. Valenti,[19] M. van Beuzekom,[31] H. Van Hecke,[66]

E. van Herwijnen,[47] C. B. Van Hulse,[17] J. van Tilburg,[31] M. van Veghel,[74] R. Vazquez Gomez,[44,22] P. Vazquez Regueiro,[45] C. Vázquez Sierra,[31] S. Vecchi,[20] J. J. Velthuis,[53] M. Veltri,[21,aa] A. Venkateswaran,[67] M. Vernet,[9] M. Veronesi,[31] M. Vesterinen,[55] J. V. Viana Barbosa,[47] D. Vieira,[5] M. Vieites Diaz,[48] H. Viemann,[73] X. Vilasis-Cardona,[44,i] A. Vitkovskiy,[31] A. Vollhardt,[49] D. Vom Bruch,[12] A. Vorobyev,[37] V. Vorobyev,[42,f] N. Voropaev,[37] R. Waldi,[73] J. Walsh,[28] J. Wang,[3] J. Wang,[71] J. Wang,[6] M. Wang,[3] Y. Wang,[7] Z. Wang,[49] D. R. Ward,[54] H. M. Wark,[59] N. K. Watson,[52] D. Websdale,[60] A. Weiden,[49] C. Weisser,[63] B. D. C. Westhenry,[53] D. J. White,[61] M. Whitehead,[13] D. Wiedner,[14] G. Wilkinson,[62] M. Wilkinson,[67] I. Williams,[54] M. Williams,[63] M. R. J. Williams,[61] T. Williams,[52] F. F. Wilson,[56] M. Winn,[11] W. Wislicki,[35] M. Witek,[33] G. Wormser,[11] S. A. Wotton,[54] H. Wu,[67] K. Wyllie,[47] Z. Xiang,[5] D. Xiao,[7] Y. Xie,[7] H. Xing,[70] A. Xu,[3] L. Xu,[3] M. Xu,[7] Q. Xu,[5] Z. Xu,[8] Z. Xu,[3] Z. Yang,[3] Z. Yang,[65] Y. Yao,[67] L. E. Yeomans,[59] H. Yin,[7] J. Yu,[7,bb] X. Yuan,[67] O. Yushchenko,[43] K. A. Zarebski,[52] M. Zavertyaev,[15,w] M. Zdybal,[33] M. Zeng,[3] D. Zhang,[7] L. Zhang,[3] S. Zhang,[3] W. C. Zhang,[3,cc] Y. Zhang,[47] A. Zhelezov,[16] Y. Zheng,[5] X. Zhou,[5] Y. Zhou,[5] X. Zhu,[3] V. Zhukov,[13,39] J. B. Zonneveld,[57] and S. Zucchelli[19,d]

(LHCb Collaboration)

[1]*Centro Brasileiro de Pesquisas Físicas (CBPF), Rio de Janeiro, Brazil*
[2]*Universidade Federal do Rio de Janeiro (UFRJ), Rio de Janeiro, Brazil*
[3]*Center for High Energy Physics, Tsinghua University, Beijing, China*
[4]*School of Physics State Key Laboratory of Nuclear Physics and Technology, Peking University, Beijing, China*
[5]*University of Chinese Academy of Sciences, Beijing, China*
[6]*Institute Of High Energy Physics (IHEP), Beijing, China*
[7]*Institute of Particle Physics, Central China Normal University, Wuhan, Hubei, China*
[8]*Univ. Grenoble Alpes, Univ. Savoie Mont Blanc, CNRS, IN2P3-LAPP, Annecy, France*
[9]*Université Clermont Auvergne, CNRS/IN2P3, LPC, Clermont-Ferrand, France*
[10]*Aix Marseille Univ, CNRS/IN2P3, CPPM, Marseille, France*
[11]*Université Paris-Saclay, CNRS/IN2P3, IJCLab, Orsay, France*
[12]*LPNHE, Sorbonne Université, Paris Diderot Sorbonne Paris Cité, CNRS/IN2P3, Paris, France*
[13]*I. Physikalisches Institut, RWTH Aachen University, Aachen, Germany*
[14]*Fakultät Physik, Technische Universität Dortmund, Dortmund, Germany*
[15]*Max-Planck-Institut für Kernphysik (MPIK), Heidelberg, Germany*
[16]*Physikalisches Institut, Ruprecht-Karls-Universität Heidelberg, Heidelberg, Germany*
[17]*School of Physics, University College Dublin, Dublin, Ireland*
[18]*INFN Sezione di Bari, Bari, Italy*
[19]*INFN Sezione di Bologna, Bologna, Italy*
[20]*INFN Sezione di Ferrara, Ferrara, Italy*
[21]*INFN Sezione di Firenze, Firenze, Italy*
[22]*INFN Laboratori Nazionali di Frascati, Frascati, Italy*
[23]*INFN Sezione di Genova, Genova, Italy*
[24]*INFN Sezione di Milano-Bicocca, Milano, Italy*
[25]*INFN Sezione di Milano, Milano, Italy*
[26]*INFN Sezione di Cagliari, Monserrato, Italy*
[27]*INFN Sezione di Padova, Padova, Italy*
[28]*INFN Sezione di Pisa, Pisa, Italy*
[29]*INFN Sezione di Roma Tor Vergata, Roma, Italy*
[30]*INFN Sezione di Roma La Sapienza, Roma, Italy*
[31]*Nikhef National Institute for Subatomic Physics, Amsterdam, Netherlands*
[32]*Nikhef National Institute for Subatomic Physics and VU University Amsterdam, Amsterdam, Netherlands*
[33]*Henryk Niewodniczanski Institute of Nuclear Physics Polish Academy of Sciences, Kraków, Poland*
[34]*AGH—University of Science and Technology, Faculty of Physics and Applied Computer Science, Kraków, Poland*
[35]*National Center for Nuclear Research (NCBJ), Warsaw, Poland*
[36]*Horia Hulubei National Institute of Physics and Nuclear Engineering, Bucharest-Magurele, Romania*
[37]*Petersburg Nuclear Physics Institute NRC Kurchatov Institute (PNPI NRC KI), Gatchina, Russia*
[38]*Institute of Theoretical and Experimental Physics NRC Kurchatov Institute (ITEP NRC KI), Moscow, Russia, Moscow, Russia*
[39]*Institute of Nuclear Physics, Moscow State University (SINP MSU), Moscow, Russia*
[40]*Institute for Nuclear Research of the Russian Academy of Sciences (INR RAS), Moscow, Russia*

[41]*Yandex School of Data Analysis, Moscow, Russia*
[42]*Budker Institute of Nuclear Physics (SB RAS), Novosibirsk, Russia*
[43]*Institute for High Energy Physics NRC Kurchatov Institute (IHEP NRC KI), Protvino, Russia, Protvino, Russia*
[44]*ICCUB, Universitat de Barcelona, Barcelona, Spain*
[45]*Instituto Galego de Física de Altas Enerxías (IGFAE), Universidade de Santiago de Compostela, Santiago de Compostela, Spain*
[46]*Instituto de Fisica Corpuscular, Centro Mixto Universidad de Valencia—CSIC, Valencia, Spain*
[47]*European Organization for Nuclear Research (CERN), Geneva, Switzerland*
[48]*Institute of Physics, Ecole Polytechnique Fédérale de Lausanne (EPFL), Lausanne, Switzerland*
[49]*Physik-Institut, Universität Zürich, Zürich, Switzerland*
[50]*NSC Kharkiv Institute of Physics and Technology (NSC KIPT), Kharkiv, Ukraine*
[51]*Institute for Nuclear Research of the National Academy of Sciences (KINR), Kyiv, Ukraine*
[52]*University of Birmingham, Birmingham, United Kingdom*
[53]*H. H. Wills Physics Laboratory, University of Bristol, Bristol, United Kingdom*
[54]*Cavendish Laboratory, University of Cambridge, Cambridge, United Kingdom*
[55]*Department of Physics, University of Warwick, Coventry, United Kingdom*
[56]*STFC Rutherford Appleton Laboratory, Didcot, United Kingdom*
[57]*School of Physics and Astronomy, University of Edinburgh, Edinburgh, United Kingdom*
[58]*School of Physics and Astronomy, University of Glasgow, Glasgow, United Kingdom*
[59]*Oliver Lodge Laboratory, University of Liverpool, Liverpool, United Kingdom*
[60]*Imperial College London, London, United Kingdom*
[61]*Department of Physics and Astronomy, University of Manchester, Manchester, United Kingdom*
[62]*Department of Physics, University of Oxford, Oxford, United Kingdom*
[63]*Massachusetts Institute of Technology, Cambridge, Massachusetts, USA*
[64]*University of Cincinnati, Cincinnati, Ohio, USA*
[65]*University of Maryland, College Park, Maryland, USA*
[66]*Los Alamos National Laboratory (LANL), Los Alamos, New Mexico, USA*
[67]*Syracuse University, Syracuse, New York, USA*
[68]*Laboratory of Mathematical and Subatomic Physics, Constantine, Algeria [associated Universidade Federal do Rio de Janeiro (UFRJ), Rio de Janeiro, Brazil]*
[69]*Pontifícia Universidade Católica do Rio de Janeiro (PUC-Rio), Rio de Janeiro, Brazil [associated Universidade Federal do Rio de Janeiro (UFRJ), Rio de Janeiro, Brazil]*
[70]*Guangdong Provencial Key Laboratory of Nuclear Science, Institute of Quantum Matter, South China Normal University, Guangzhou, China (associated Center for High Energy Physics, Tsinghua University, Beijing, China)*
[71]*School of Physics and Technology, Wuhan University, Wuhan, China (associated Center for High Energy Physics, Tsinghua University, Beijing, China)*
[72]*Departamento de Fisica, Universidad Nacional de Colombia, Bogota, Colombia (associated LPNHE, Sorbonne Université, Paris Diderot Sorbonne Paris Cité, CNRS/IN2P3, Paris, France)*
[73]*Institut für Physik, Universität Rostock, Rostock, Germany (associated with Physikalisches Institut, Ruprecht-Karls-Universität Heidelberg, Heidelberg, Germany)*
[74]*Van Swinderen Institute, University of Groningen, Groningen, Netherlands (associated Nikhef National Institute for Subatomic Physics, Amsterdam, Netherlands)*
[75]*National Research Centre Kurchatov Institute, Moscow, Russia [associated Institute of Theoretical and Experimental Physics NRC Kurchatov Institute (ITEP NRC KI), Moscow, Russia, Moscow, Russia)]*
[76]*National University of Science and Technology "MISIS", Moscow, Russia [associated Institute of Theoretical and Experimental Physics NRC Kurchatov Institute (ITEP NRC KI), Moscow, Russia, Moscow, Russia]*
[77]*National Research University Higher School of Economics, Moscow, Russia (associated Yandex School of Data Analysis, Moscow, Russia)*
[78]*National Research Tomsk Polytechnic University, Tomsk, Russia [associated Institute of Theoretical and Experimental Physics NRC Kurchatov Institute (ITEP NRC KI), Moscow, Russia, Moscow, Russia]*
[79]*University of Michigan, Ann Arbor, Michigan, USA (associated Syracuse University, Syracuse, New York, USA)*

[a]Deceased.
[b]Also at Laboratoire Leprince-Ringuet, Palaiseau, France.
[c]Also at Università di Genova, Genova, Italy.
[d]Also at Università di Bologna, Bologna, Italy.

[e]Also at Università di Modena e Reggio Emilia, Modena, Italy.
[f]Also at Novosibirsk State University, Novosibirsk, Russia.
[g]Also at Università di Ferrara, Ferrara, Italy.
[h]Also at Università di Milano Bicocca, Milano, Italy.
[i]Also at DS4DS, La Salle, Universitat Ramon Llull, Barcelona, Spain.
[j]Also at Università di Pisa, Pisa, Italy.
[k]Also at Universidad Nacional Autonoma de Honduras, Tegucigalpa, Honduras.
[l]Also at Università di Bari, Bari, Italy.
[m]Also at Università di Cagliari, Cagliari, Italy.
[n]Also at INFN Sezione di Trieste, Trieste, Italy.
[o]Also at Università degli Studi di Milano, Milano, Italy.
[p]Also at Universidade Federal do Triângulo Mineiro (UFTM), Uberaba-MG, Brazil.
[q]Also at AGH—University of Science and Technology, Faculty of Computer Science, Electronics and Telecommunications, Kraków, Poland.
[r]Also at Università di Siena, Siena, Italy.
[s]Also at Università di Padova, Padova, Italy.
[t]Also at Scuola Normale Superiore, Pisa, Italy.
[u]Also at MSU—Iligan Institute of Technology (MSU-IIT), Iligan, Philippines.
[v]Also at Hanoi University of Science, Hanoi, Vietnam.
[w]Also at P.N. Lebedev Physical Institute, Russian Academy of Science (LPI RAS), Moscow, Russia.
[x]Also at Università di Roma Tor Vergata, Roma, Italy.
[y]Also at Università della Basilicata, Potenza, Italy.
[z]Also at Università di Roma La Sapienza, Roma, Italy.
[aa]Also at Università di Urbino, Urbino, Italy.
[bb]Also at Physics and Micro Electronic College, Hunan University, Changsha City, China.
[cc]Also at School of Physics and Information Technology, Shaanxi Normal University (SNNU), Xi'an, China.